RAA 2018 Vol. **18** No. **11**, 144(12pp) doi: 10.1088/1674–4527/18/11/144

http://www.raa-journal.org *http://iopscience.iop.org/raa*

***R**esearch in*
***A**stronomy and*
***A**strophysics*

Color gradients of the galaxies at $0.5 < z < 1$ II. Clustering properties

Zhi-Xiong Liang[1,2] and Cheng Li[3]

[1] Shanghai Astronomical Observatory, Chinese Academy of Sciences, Shanghai 200030, China; *zliang18@ustc.edu.cn*

[2] University of Chinese Academy of Sciences, Beijing 100049, China

[3] Tsinghua Center for Astrophysics and Physics Department, Tsinghua University, Beijing 100084, China

Received 2018 May 14; accepted 2018 May 21

Abstract We investigate the dependence of clustering on luminosity, stellar mass and color gradient for galaxies at $0.5 < z < 1$, using a sample of ~ 6300 galaxies from the final data release of the VIMOS Public Extragalactic Redshift Survey (VIPERS-PDR2). We estimate both the auto-correlation function for galaxy samples selected by B-band absolute magnitude and stellar mass, and the cross-correlation function of galaxy samples selected by color gradient with respect to the full galaxy sample. The auto-correlation function amplitudes at fixed scale are found to positively correlate with both galaxy luminosity and stellar mass, and the effect holds for all the scales probed ($0.2\,h^{-1}\,\mathrm{Mpc} < r_\mathrm{p} < 20\,h^{-1}\,\mathrm{Mpc}$), in good agreement with previous measurements based on an earlier data release of VIPERS. When the stellar mass is limited to a narrow range, we find the clustering power to be essentially independent of galaxy color gradient, and this conclusion is true for all the masses and all the scales considered here. In a parallel paper, we find that the half-light radius is the only galaxy property other than stellar mass that is related to color gradient. Considering the previous finding that clustering depends weakly on galaxy structure at given mass, the non-dependence of clustering on color gradient found here reinforces our conclusion that the color gradient and structural parameters of a galaxy are intrinsically related to each other.

Key words: galaxies: photometry — galaxies: statistics — galaxies: evolution

1 INTRODUCTION

Most of our knowledge on the large-scale structure of the Universe comes from the studies of large redshift surveys of nearby galaxies, such as the Two-degree Field Galaxy Redshift Survey (2dFGRS Colless et al. 2001) and Sloan Digital Sky Survey (SDSS; York et al. 2000). Thanks to these surveys, the clustering of galaxies as a function of their physical properties has been investigated with unprecedented accuracy, as is usually quantified by the two-point correlation function (2PCF) (Peebles 1980).

These studies have clearly established that galaxy clustering depends on a variety of galaxy properties. These include luminosity (White et al. 1988; Zehavi et al. 2005; Wang et al. 2007; Meneux et al. 2008, 2009; Zehavi et al. 2011; Marulli et al. 2013; Guo et al. 2013), stellar mass (Li et al. 2006a; Wang et al. 2008; Meneux et al. 2008, 2009; Marulli et al. 2013), color (Willmer et al. 1998; Zehavi et al. 2005, 2011; Li et al. 2006a; Wang et al. 2008; Guo et al. 2013), morphological or spectral type (Norberg et al. 2002; Madgwick et al. 2003; Wang et al. 2007), structural parameters such as concentration index and surface stellar mass density (Goto et al. 2003; Li et al. 2006a), the 4000 Å break (Li et al. 2006a), star formation and nuclear activities (Li et al. 2008a,b). Generally, galaxies are more strongly clustered if they have higher luminosities and stellar masses, redder colors, early-type morphologies and older stellar populations.

In addition to the global properties, spatially resolved properties are also expected to provide interesting information about the evolution processes of galaxies, because the star formation history may vary across a galaxy with different star formation status at different radii. Radial color gradient is one such property, which is a combined result of the radial gradient in the stellar population properties including age, metallicity, surface mass density and dust attenuation. Color is just an indicator of the stellar population at a given radius, and it may be affected by dust extinction. However, color gradient is still useful in many cases, especially when spatially resolved spectroscopy is not available for large samples of galaxies.

In this work, we attempt to study the clustering of galaxies at intermediate redshifts as a function of their color gradient, using a sample of 6300 galaxies at $0.5 < z < 1$ with spectroscopy from the VIMOS Public Extragalactic Redshift Survey (VIPERS, Guzzo et al. 2014; Scodeggio et al. 2018)[1] and multi-band photometry from the VIPERS-Multi-Lambda Survey (VIPERS-MLS, Moutard et al. 2016a,b)[2]. This redshift range is the cosmic epoch when star formation activity in galaxies was still rapidly declining, thus it is an epoch important for the buildup of the quiescent galaxy population, which has become a majority population of the local Universe. The star formation cessation process has been the driving factor in galaxy evolution over the past ~ 8 Gyr. The physical mechanisms behind this evolution process, however, remain unclear. Both internal processes and environmental effects external to galaxies are expected to play varying roles in the star formation cessation process.

In a parallel paper (Liang & Li 2018, hereafter Paper I) we have estimated a variety of physical properties for the VIPERS galaxies using the VIPERS-PDR2 and VIPERS-MLS data including stellar mass, half-light radius, rest-frame luminosities in different bands and star formation rate (SFR). In addition, we selected galaxies with substantially good spatial resolution and estimate a two-zone color, defined by the difference in rest-frame $(u - r)$ color between the outer and inner region. We compared the global properties for the galaxies with negative color gradients ("red-cored" galaxies) and those with positive color gradients ("blue-cored" galaxies). We found that when stellar mass is limited to a certain range, the only galaxy property that is related with color gradient is the half-light radius, implying that the color gradient and structural parameters of galaxies are intrinsically correlated. In this work, we will extend this to study the clustering of galaxies with different color gradients, employing the same sample as used in Paper I.

This paper is organized in the following manner. In Section 2, we describe the VIPERS galaxy sample and our clustering estimators. In Section 3, we present the clustering measurements for galaxies of different stellar mass and luminosity bins, as well as the clustering measurements for galaxies with red cores and blue cores. We summarize our work in the final section.

Throughout this paper, we assume a flat ΛCDM cosmology with $\Omega_m = 0.30, \Omega_\Lambda = 0.70, H_0 = 70\,\mathrm{km\,s^{-1}\,Mpc^{-1}}$ and $h = H_0/100$. All magnitudes are given in the AB system (Oke & Gunn 1983) and corrected for Galactic extinction following Schlegel et al. (1998).

2 DATA AND METHODOLOGY

2.1 The VIPERS Galaxy Sample and Physical Properties

VIPERS (Guzzo et al. 2014; Scodeggio et al. 2018) is a large redshift survey carried out with the VIMOS spectrograph at the 8.2 m Very Large Telescope. VIPERS obtained high-quality spectroscopy for more than 90 000 galaxies at $0.5 < z < 1.2$ with i-band AB magnitude down to $i = 22.5$, covering a total sky area of 23.5 deg^2. The VIPERS footprint consists of two separate fields, which are the W1 and W4 fields of the Canada-France-Hawaii Telescope Legacy Survey (CFHTLS, Cuillandre et al. 2012). Multi-band deep imaging is available for the VIPERS fields over a wide wavelength range from VIPERS-MLS (Moutard et al. 2016a,b)[3]. These include the five optical bands $ugriz$ from CFHTLS, far-ultraviolet (FUV) and/or near-ultraviolet (NUV) from *Galaxy Evolution Explorer* (*GALEX*, Martin et al. 2005), and the Ks band from WIRcam (Thibault et al. 2003).

The VIPERS selected galaxy targets based on color-color diagrams, yielding a high sampling rate of $\sim 50.1\%$ and a success rate of reliable redshift measurements of $\sim 84.3\%$. In this work, we consider the redshift range of $0.5 < z < 1.0$ and require a galaxy to be reliably measured with a redshift in order to be included in our sample. This gives rise to a sample of 62 985 galaxies with $0.5 < z < 1$, distributed over an

[1] *http://vipers.inaf.it*

[2] *http://cesam.lam.fr/vipers-mls*

[3] *http://cesam.lam.fr/vipers-mls*

effective area of 16.3 deg^2 after photometric and spectroscopic masks are taken into account. About half of our galaxies has FUV/NUV, u, g, r, i, z, Ks photometry, and the other half has u, g, r, i, z, Ks only.

As described in Paper I, we have fitted the spectral energy distribution (SED) from the VIPERS-MLS photometry using the public code `CIGALE` (Noll et al. 2009), and estimated a variety of physical properties for each galaxy in our sample. These include stellar mass M_*, rest-frame colors such as $u-r$, $g-r$ and $r-Ks$, half-light radius $R50$ (the radius enclosing half of the total light in the i-band) and SFR. We have also estimated a two-zone color defined as the difference in $u-r$ between the outer region ($R50 < R < R80$) and the inner region ($R < R20$), where $R20$ and $R80$ are the radii enclosing 20% and 80% of the total light in the i-band respectively. According to $\Delta(u-r)$, we select galaxies with either a "red core" or a "blue core," by requiring $\Delta(u-r)$ to be outside the 1σ region of the median $\Delta(u-r)$ for galaxies at a given stellar mass. Those with negative $\Delta(u-r)$ are classified as "red-cored" galaxies because of their relatively red colors in the inner region, and those with positive $\Delta(u-r)$ are classified as "blue-cored" galaxies because of their relatively blue colors in the outer region. The reader is referred to Paper I for a detailed description of our methodology for obtaining the galaxy properties and the associated classification.

Figure 1 displays the distribution of our galaxies on the plane of B-band absolute magnitude versus redshift (left panel) and the plane of stellar mass versus redshift (right panel). We have corrected the average redshift evolution of the luminosity by $M_B(z) = M_B(0) - z$, following previous studies (Ilbert et al. 2005; Meneux et al. 2009; Marulli et al. 2013). The figure shows that the sample is a typical magnitude-limited sample. The redshift-dependent faint limit in M_B corresponds to the i-band limiting magnitude of the survey, which is $i = 22.5$. Due to this "volume effect," the sample is biased to brighter galaxies at higher redshifts, and one would have to exclude faint galaxies with low masses in order to have a volume-selected sample which is complete over the survey volume for a relatively bright luminosity or mass threshold. For instance, according to Figure 1, our sample is complete down to a stellar mass of $M_* \sim 10^{10}$ or a B-band absolute magnitude of $M_B \sim -20.5$.

2.2 Clustering Estimator

We quantify the clustering of the VIPERS galaxy sample by measuring the 2PCF. We will divide our galaxies into subsamples according to M_B and M_* in order to study the dependence of clustering on luminosity and mass. For a given luminosity or mass subsample, we will further divide the galaxies into subsets of galaxies that are either "red-cored" or "blue-cored," thus examining the clustering properties of galaxies with different color gradients. We estimate both the auto-correlation function for a given subsample of galaxies and the cross-correlation of the subsample with respect to the full sample.

A random sample must be constructed for the estimator, and it must be randomly distributed with the same angular and radial selection function as the galaxy sample. We have constructed a random sample which has the same selection effects as our VIPERS galaxy sample. We have applied the photometric and spectroscopic masks of VIPERS-PDR2[4] to have the same survey geometry in both of the VIPERS fields. We adopt the $V_{\rm max}$ smoothed radial distribution to take into account the redshift-dependent selection effect (Kovač et al. 2010; de la Torre et al. 2013).

Given the random sample (`Sample R`) and a galaxy sample (`Sample D`), we first estimate the auto-correlation function in redshift space, $\xi(r_{\rm p}, \pi)$, using the Landy & Szalay (1993) estimator

$$\xi(r_{\rm p}, \pi) = \frac{DD(r_{\rm p}, \pi) - 2DR(r_{\rm p}, \pi) + RR(r_{\rm p}, \pi)}{RR(r_{\rm p}, \pi)} \ . \tag{1}$$

Here, $r_{\rm p}$ and π are the projected separation and the line-of-sight separation, respectively. $DD(r_{\rm p}, \pi)$ is the galaxy-galaxy pair count with separations $\log_{10} r_{\rm p} \pm 0.5\Delta \log_{10} r_{\rm p}$ and $\pi \pm 0.5\Delta\pi$. $DR(r_{\rm p}, \pi)$ and $RR(r_{\rm p}, \pi)$ are respectively the galaxy-random and random-random pair counts.

The projected auto-correlation function $w_{\rm p}(r_{\rm p})$ is then estimated by integrating $\xi(r_{\rm p}, \pi)$ along the line of sight, given by

$$w_{\rm p}(r_{\rm p}) = 2\int_0^\infty \xi(r_{\rm p}, \pi) d\pi = 2\sum_i \xi(r_{\rm p}, \pi_i)\Delta\pi_i \ . \tag{2}$$

The integration runs from $\pi = h^{-1}\,{\rm Mpc}$ to $\pi = 39.5\,h^{-1}\,{\rm Mpc}$, with $\Delta\pi_i = 1\,h^{-1}\,{\rm Mpc}$ following common practice.

For a given subsample of galaxies (`Sample Q`), we also estimate a projected cross-correlation function with respect to the full galaxy sample (`Sample D`). Again, we start by estimating the redshift-space corre-

[4] *http://vipers.inaf.it/rel-pdr2.html*

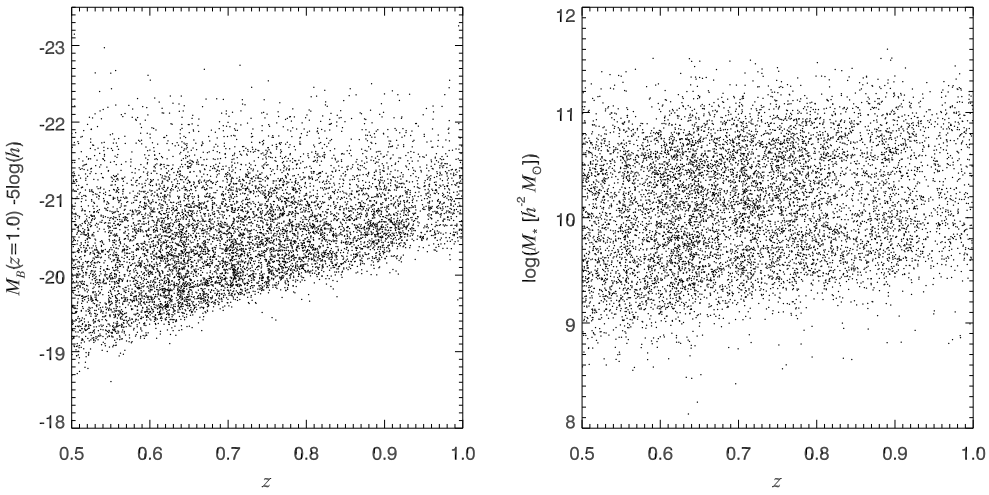

Fig. 1 Distribution of our galaxy sample on the plane of B-band absolute magnitude versus redshift (*left panel*), and the plane of stellar mass versus redshift (*right panel*). A random subset of 15% galaxies from the whole sample is plotted in order to reduce plot file size.

lation function, but using the following estimator

$$\xi(r_{\rm p},\pi) = \frac{QD(r_{\rm p},\pi)}{QR(r_{\rm p},\pi)} - 1 \ , \qquad (3)$$

where $QD(r_{\rm p},\pi)$ and $QR(r_{\rm p},\pi)$ are the cross pair counts between `Sample Q` and `Sample D`, and between `Sample Q` and the random sample `Sample R`. The corresponding projected cross-correlation function, $w_{\rm p}(r_{\rm p})$, is then obtained by Equation (2) as above.

We have applied the slit corrections following Marulli et al. (2013, hereafter M13) which are derived by calculating the ratio between the redshift-space 2PCF measured in mock catalogs with and without applying the slit mask target mask selection algorithm. When estimating the pair counts used in the clustering estimators, we add up the pair counts from the W1 and W4 fields to have the total pair counts, weighting the counts of each field by its real sample size. Errors in the correlation functions are estimated using the bootstrap resampling technique (Barrow et al. 1984).

3 RESULTS

3.1 Luminosity and Mass Dependence of the Auto-Correlations

Figure 2 shows the redshift-space two-point auto-correlation function, $\xi(s)$, for galaxies in different luminosity and mass bins. Here, the correlation function $\xi(s)$ is measured using the same estimator as $\xi(r_{\rm p},\pi)$ in Equation (1), but as a function of the three-dimensional separation in redshift space, $s = \sqrt{r_{\rm p}^2+\pi^2}$. The VIPERS galaxy sample is split into different subsamples according to B-band absolute magnitude (M_B) or stellar mass, and we estimate $\xi(s)$ for each subsample. The upper panels in Figure 2 show the results for the subsamples selected by M_B and the lower panels are for the M_* subsamples. We consider two successive redshift ranges, $0.5 < z < 0.7$ and $0.7 < z < 0.9$, and show the results of the two ranges separately in the left and right panels.

In Figure 3 we show the projected auto-correlation functions, $w_{\rm p}(r_{\rm p})$, measured for the same set of subsamples and redshift ranges as in the previous figure. For comparison, in both figures we also show the measurements from M13, as plotted in open circles connected by dotted lines, which are based on VIPERS-PDR1 and measured for the same M_B and M_* intervals as adopted here. As can be seen, our measurements agree very well with theirs, with the $\xi(s)$ and $w_{\rm p}(r_{\rm p})$ overlapping with each other in most cases. There are some differences occurring at the largest scales probed ($s \gtrsim 20\,h^{-1}\,{\rm Mpc}$ and $r_{\rm p} \gtrsim 10\,h^{-1}\,{\rm Mpc}$). However, these differences are not significant given the large error bars at those large scales, and so should not be overemphasized. The comparisons presented in the two figures indicate that we have fully understood the selection effects of the VIPERS sample and successfully reproduced the clustering measurements, at least for scales below $\sim 10-20\,h^{-1}\,{\rm Mpc}$. In what follows, we will focus on these scales and ignore the clustering measurements above $20\,h^{-1}\,{\rm Mpc}$.

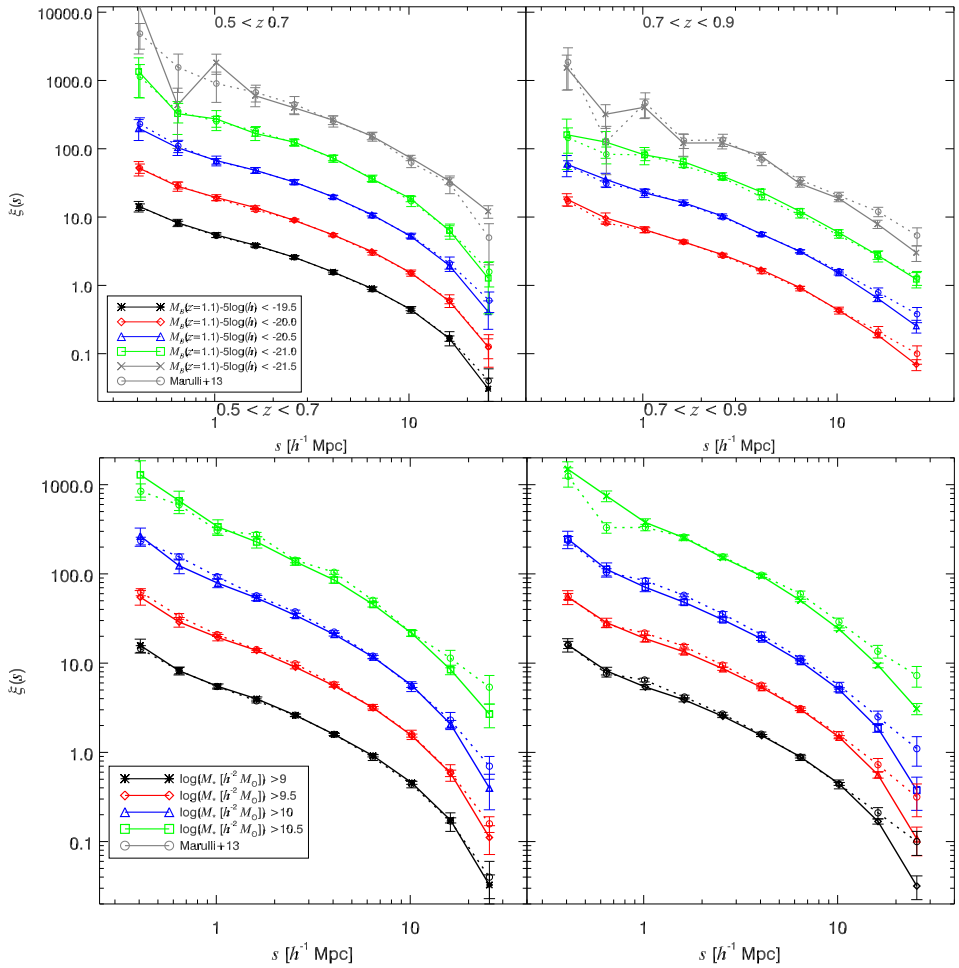

Fig. 2 Two-point auto-correlation function of the VIPERS galaxies in different intervals of B-band absolute magnitude (*upper panels*) and stellar mass intervals (*bottom panels*). Left and right panels are results for two redshift ranges as indicated. In each panel, the *colored solid symbols*/*lines* represent our measurements, while the *open circles* connected by *dotted lines* are the measurements carried out by M13 with data from VIPERS-PDR1. The results in different sub-samples are offset by 0.5 dex from the lower luminosity and stellar mass sub-samples, for visual clarity.

Figure 2 shows clear suppression of the clustering power on small scales, a known effect which is caused by the peculiar motions of galaxies. One would expect the 2PCF to be more linearly dependent on galaxy-galaxy separation in real space, and this is indeed the case as can be seen from projected 2PCFs shown in Figure 3, where $w_{\rm p}$ decreases with $r_{\rm p}$ almost linearly in log-log space. Following previous studies, we fit the $w_{\rm p}(r_{\rm p})$ measurements with a power-law model, over the $r_{\rm p}$ interval of $0.2 < r_{\rm p}[\,h^{-1}\,{\rm Mpc}] < 20$. We do not consider the largest scales for the reason mentioned above. The data points at smallest scales ($r_{\rm p} < 0.2\,h^{-1}\,{\rm Mpc}$) are also excluded due to their relatively large errors. The power-law fits are shown in the figure as solid lines. Generally, the model can describe the measurements of $w_{\rm p}(r_{\rm p})$ well.

In conclusion, the analysis in the current subsection aims to show that we have fully understood the sample selections and are able to reproduce the clustering measurements as a function of both luminosity and stellar mass, which are in good agreement with the measurements published in previous studies. The luminosity and mass dependence of the auto-correlation function are similar to what have been observed for lower redshift galaxies, such as from SDSS. It would be interesting to compare measurements from the VIPERS sample and those from SDSS, which should be able to provide a better understanding of the evolution of the galaxy clustering from $z = 1$ down to the present day. These measurements and comparisons should also be able to provide interesting constraints on galaxy formation and evolution

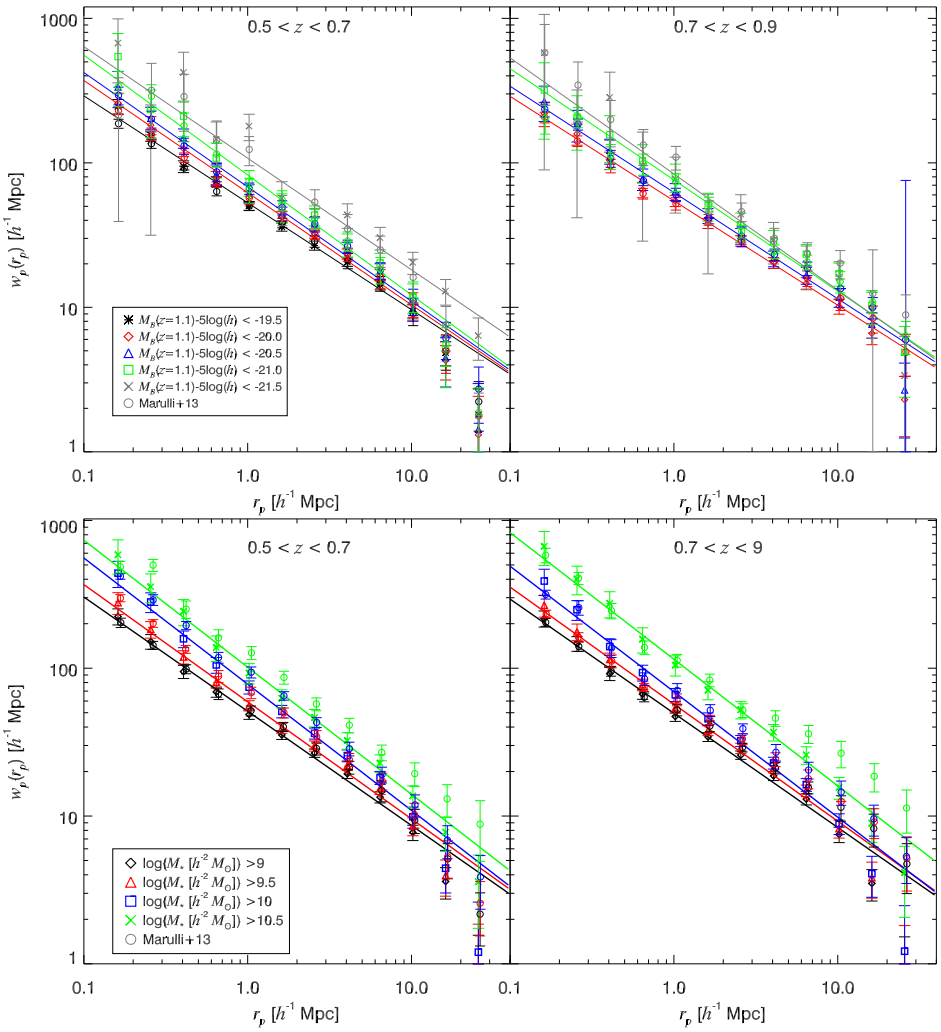

Fig. 3 Projected 2PCF of VIPERS-PDR2 galaxies as a function of B-band absolute magnitude (*top panels*) and stellar mass (*bottom panels*). The *open circles* in corresponding color are results of VIPERS-PDR1 from M13, with $r_{\rm p}$ slightly shifted for clarity. The *solid lines* show the power-law best-fits, obtained by fitting the projected 2PCF in the interval $0.2 < r_{\rm p}[\,h^{-1}\,{\rm Mpc}] < 20$. Results from M13 are plotted in *open circles* for comparison.

models, if compared to theoretical models or numerical simulations of galaxy formation. In the current work, we are interested in comparing the clustering properties for galaxies with different color gradients, and will leave the comparisons with low-z measurements and models to future studies.

3.2 Dependence of Clustering on Color Gradients

In this section, we examine the dependence of clustering of galaxies on their color gradients. In Paper I, we have estimated the color gradient of each galaxy in our sample, quantified by two parameters: a two-zone color in rest-frame $\Delta(u-r)$ defined as the difference in $(u-r)$ between the outer region ($R50 < R < R80$) and inner region ($R < R20$), and the radius-scaled color gradient G_{ur} defined by the ratio of $\Delta(u-r)$ to $0.5(R50+R80)$. We found that, although the galaxies in our sample show a nearly flat color gradient on average, the distribution of both $\Delta(u-r)$ and G_{ur} at fixed mass actually spans a wide range. This means that many galaxies present either a positive color gradient (bluer center and redder outskirt) or a negative color gradient (redder center and bluer outskirt). We have selected two subsets of galaxies with either a "red core" or a "blue core," by requiring them to have significantly negative or positive $\Delta(u-r)$, falling beyond the 1σ region of the median relation between $\Delta(u-r)$ and stellar mass. Comparisons of a variety of galaxy properties between the "red-cored" and

"blue-cored" galaxy subsamples revealed that the only galaxy property other than stellar mass that is correlated with color gradient is the half-light size ($R50$), with massive red-cored galaxies being larger than massive blue-cored galaxies when stellar mass is limited to a narrow range.

In this paper, we further compare the clustering properties of the "red-cored" and "blue-cored" galaxy samples. As mentioned in Paper I, we have constructed two galaxy samples from the VIPERS full sample, `Sample S0.55` including galaxies with $R50/\mathrm{PSF_{fwhm}} > 0.55$ and `Sample S1.0` including galaxies with $R50/\mathrm{PSF_{fwhm}} > 1$. Here $\mathrm{PSF_{fwhm}}$ is the full-width at half maximum (FWHM) of the point spread function (PSF) for the VIPERS imaging data in the i-band. These limits ensure a substantially good spatial resolution for measuring the two-zone color. On the other hand, however, these limits complicate the selection effects of the red-cored and blue-cored galaxy samples, which are hard to be accurately taken into account when we construct the random sample. Furthermore, these limits also significantly reduce the sample size. Therefore, we choose not to directly measure the auto-correlation function for a given red-cored or blue-cored subsample. Instead, for a given subsample, we measure the cross-correlation function with respect to a reference sample which is actually the full galaxy sample from VIPERS (see Eq. (3)). One of the advantages of cross-correlation functions is that one can obtain clustering measurements with high signal-to-noise ratios even for a small sample, thanks to the large size of the reference sample (e.g. Li et al. 2006b).

Figure 4 displays the $w_{\rm p}(r_{\rm p})$ measurements for five stellar mass intervals, as indicated in each panel. Each panel shows the results for a given stellar mass interval, and in each panel the red and blue symbols/lines present the results for the "red-cored" and "blue-cored" galaxies falling in the corresponding mass range. For comparison, we also display the results for the galaxies that have a $\Delta(u-r)$ within the 1σ range of the median $\Delta(u-r)$ for their stellar mass, as plotted in green symbols/lines. In the lower panels, we show the ratio of the "red-cored" (red symbols/lines) and the "blue-cored" (blue symbols/lines) subsamples relative to the median subsample. In each stellar mass range, we have matched the red-cored and blue-cored subsamples so as to have the same stellar mass distribution. By doing so, we make sure that the clustering differences (if any) would be a real signature of the color gradient dependence on clustering.

It is clear from this figure that the projected cross-correlation function $w_{\rm p}(r_{\rm p})$ is almost identical for the different subsamples at given mass, with no significant differences at all scales probed. This strongly indicates that the internal color gradient for galaxies with similar mass is not related to environmental effects occurring at different scales.

In Figure 5, we repeat the analysis as presented in the previous figure, but for different stellar mass thresholds instead of differential mass bins. For a given threshold, we include all the galaxies with stellar mass exceeding the threshold and estimate the projected cross-correlation function with the reference sample in the same way as described above.

Figure 5 shows that, as expected, the errors of the $w_{\rm p}(r_{\rm p})$ measurements are reduced when compared to the measurements in the previous figure, because of the larger sample size at the given mass threshold. However, the subsamples of different color gradients still show the same clustering behaviors, at all the scales and at all mass thresholds.

Next, we examine the potential effect of the limit in galaxy size which we adopt to select our galaxies in `Sample S0.55`, i.e. the parent sample employed for the analyses above. To this end, we use `Sample S1.0` instead of `Sample S0.55` and estimate the projected cross-correlations for the same sets of subsamples selected by mass thresholds. The measurements are presented in Figure 6 where the symbols/lines are exactly the same as in the previous figure. Although the measurements become more noisy due to the smaller sample size, our conclusion remains that there is no significant difference in clustering at all scales when comparing the galaxies with similar mass but different color gradients.

Previous studies have established that, in addition to stellar mass (and luminosity of a given band), other properties such as global colors and structural parameters (e.g., concentration) may also be related to environment (e.g., Li et al. 2006a; Blanton & Moustakas 2009). In order to examine the potential effect on our results, for a given mass interval or threshold, we have further matched the subsamples of red-cores and blue-cores in global color and concentration, finding the clustering amplitudes to remain undistinguished.

Finally, in Figure 7 we compare the measurements of projected cross-correlation function for red-cored and blue-cored galaxies, for the same set of mass intervals

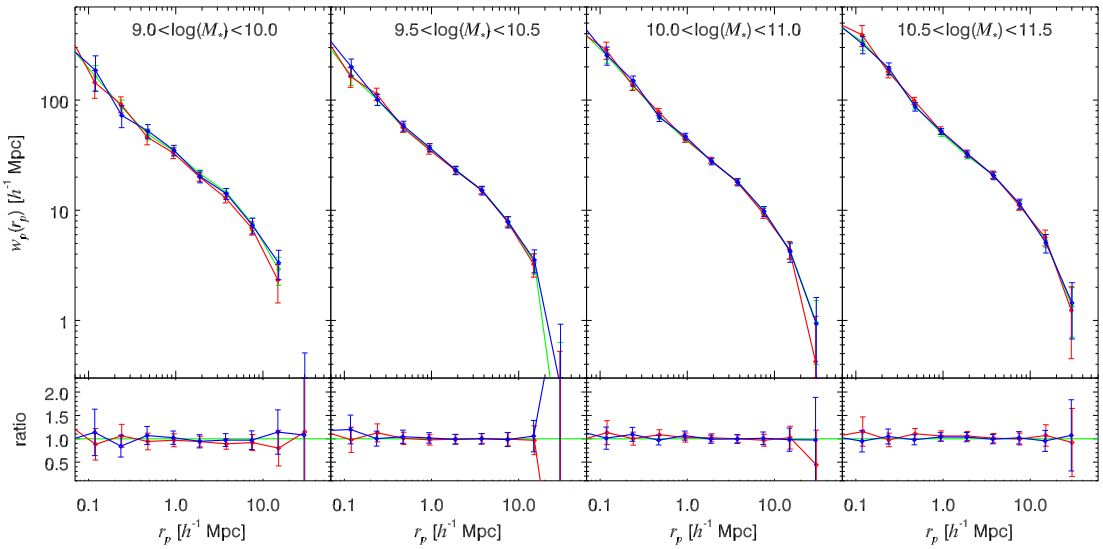

Fig. 4 Projected cross-correlation function $w_{\rm p}(r_{\rm p})$, as a function of projected separation $r_{\rm p}$, is measured for galaxies in different stellar mass intervals and with different color gradients. Panels from left to right are for different stellar mass ranges as indicated in each panel. In each panel, the *red* and *blue symbols* are for subsets of galaxies with red or blue cores, while the *green symbols* are for galaxies with flat/weak gradients. The lower panels display the ratio of $w_{\rm p}(r_{\rm p})$ measured for the red-/blue-cored galaxy sample relative to that for the sample of median gradients. See the text for detailed description of the subsample selection.

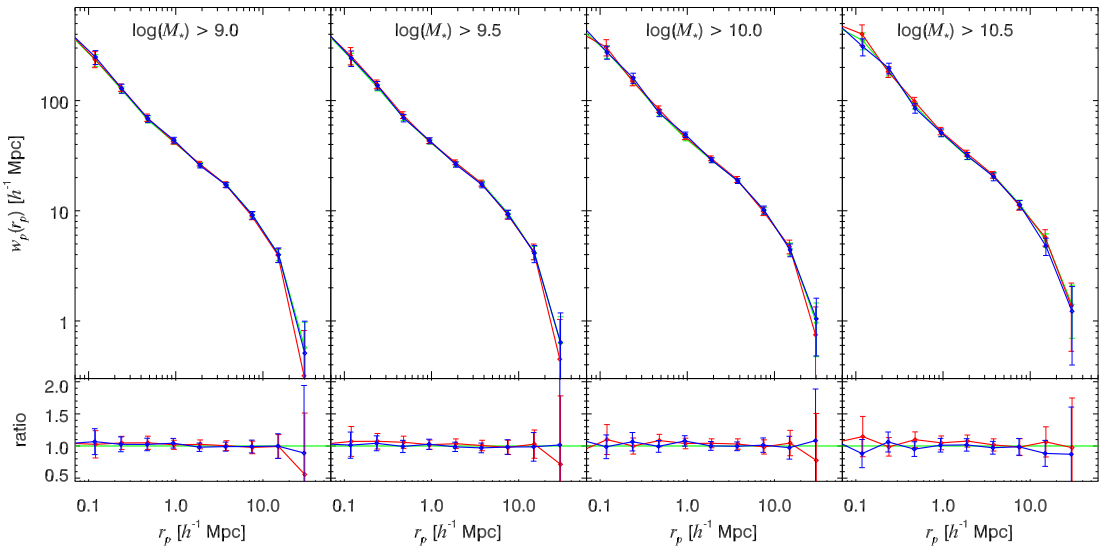

Fig. 5 Projected cross-correlation function $w_{\rm p}(r_{\rm p})$, as a function of projected separation $r_{\rm p}$, is measured for galaxies above different stellar mass thresholds (as indicated in each panel) and with different color gradients. Symbols/lines are the same as in Fig. 4.

and mass thresholds, but defining the color gradient using $(g-r)$ instead of $(u-r)$. The $(g-r)$ color index has been widely investigated in previous studies of galaxy clustering (e.g. Li et al. 2006a). The upper panels of the figure show the results of different mass intervals, while the lower panels are for different mass thresholds, with the same symbols/lines as in Figures 4 and 5. Overall, we do not see any significant differences between the subsamples of different color gradients at a given mass range or threshold. At lowest masses with $9 < \lg(M_*/M_\odot) < 10$, the red-cored galaxy sample appears to be more strongly clustered at intermediate scales ($r_{\rm p}$ at a few $\times 100\,h^{-1}$ kpc), but the effect is not significant at all given the overlapping error bars.

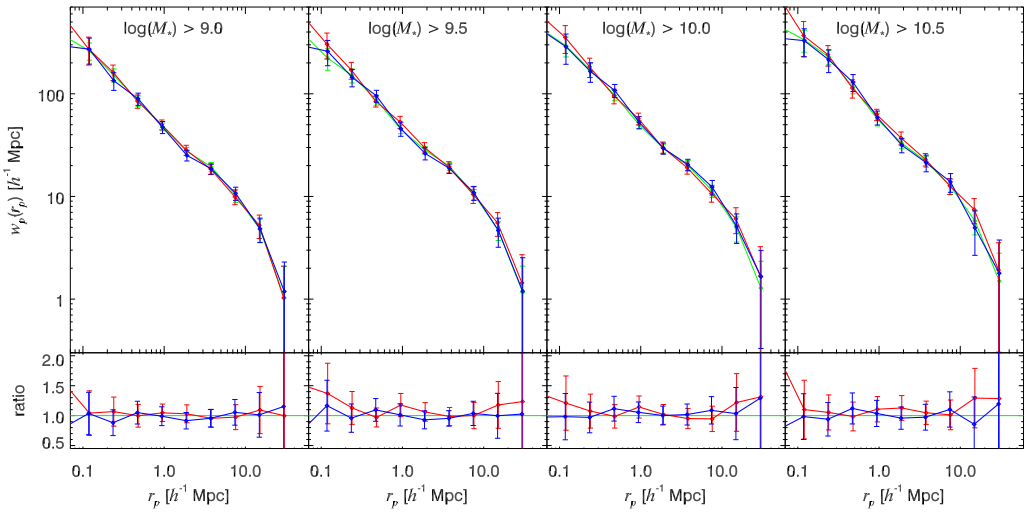

Fig. 6 Same as Fig. 5, but for the galaxy sample `Sample S1.0` instead of `Sample S0.55`.

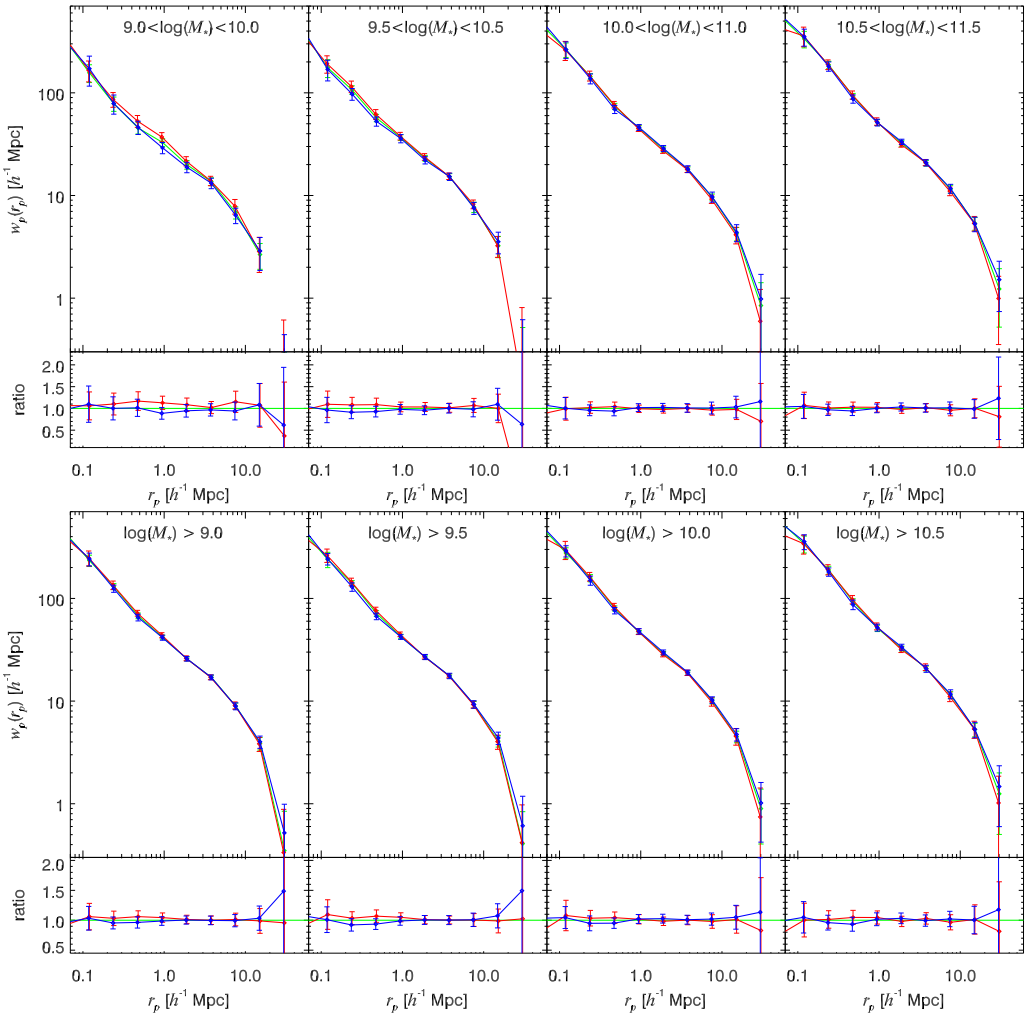

Fig. 7 *Upper panels:* Projected cross-correlation function $w_{\rm p}(r_{\rm p})$ for galaxies in different stellar mass intervals as indicated in each panel. Different colors/symbols are for subsets of galaxies with different color gradients as in previous figures, but the color gradients are measured with $(g-r)$ instead of $(u-r)$. *Lower panels:* same as upper panels but for mass thresholds instead of differential mass bins, as indicated in each panel.

Therefore, we conclude that galaxy clustering does not depend on the color gradient of galaxies when stellar mass is limited to a narrow range, and this is true for all masses and at all scales from $\sim 0.2\,h^{-1}\,\mathrm{Mpc}$ up to $\sim 20\,h^{-1}\,\mathrm{Mpc}$.

4 SUMMARY

In this paper, we have investigated the clustering properties for galaxies of different color gradients, selected from a parent sample of 62 985 galaxies at $0.5 < z < 1$ from the final data release of the VIPERS survey (VIPERS-PDR2). We have classified our galaxies as either "red-cored" or "blue-cored" by requiring the two-zone color $\Delta(u-r)$ to be significantly negative or positive. We then estimate the projected cross-correlation function $w_{\rm p}(r_{\rm p})$ for subsamples of red-cored and blue-cored galaxies, both limited to narrow ranges of stellar mass, with respect to the full galaxy sample. We have also estimated the redshift space and projected auto-correlation functions for samples selected by B-band absolute magnitude and stellar mass, and compared the results with previous studies, finding good agreement.

Our conclusions regarding the clustering properties of galaxies with different color gradients can be summarized in one sentence, that is, we find no dependence of galaxy clustering on galaxy color gradient when the samples of different color gradients are matched in stellar mass. This conclusion holds for all the stellar masses and for all scales probed, ranging from $\sim 0.2\,h^{-1}\,\mathrm{Mpc}$ up to $\sim 20\,h^{-1}\,\mathrm{Mpc}$. We have repeated the same analysis for color gradients defined with $g-r$ instead of $u-r$, and for galaxies with photometry acquired with better spatial resolution. The same results and conclusions remain unchanged in any case.

It is worth comparing our results with many studies that have examined environmental dependence of color gradients. Most studies have focused on early-type galaxies (ETGs) at $z < 0.2$ based on photometric data (e.g., Ko & Im 2005; La Barbera et al. 2005, 2011; Tortora & Napolitano 2012). These studies have revealed that, statistically, ETGs associated with a dense environment (e.g., groups or clusters of galaxies with high richness) present weak color gradients compared to ETGs in low-density regions, and this effect is believed to be driven by metallicity (Saglia et al. 2000; Ferreras et al. 2009; Spolaor et al. 2010). On the other hand, however, photometric studies of ETGs revealed no environmental dependence of color gradient (e.g., Tamura & Ohta 2000). Recent observations of integral field spectroscopy (IFS) have provided radial profiles of both age and metallicity for large samples of nearby galaxies, including both early-type and late-type galaxies. These observations have allowed the correlation of age and metallicity gradients with environment to be studied with high accuracy. For instance, using the IFS data from the Mapping Nearby Galaxies at Apache Point Observatory (MaNGA, Bundy et al. 2015), Goddard et al. (2017) examined the dependence of age/metallicity gradients with local density, while Zheng et al. (2017) further examined the correlation with large-scale structure type and central/satellite classification. Both studies found no/weak correlations. Our results obtained from $0.5 < z < 1$ are apparently very consistent with these previous studies of low-z galaxies.

Perhaps it is not surprising to find no dependence of clustering on color gradient. In Paper I, we find that color gradient is mainly dependent on stellar mass, with negative color gradients in massive galaxies. In addition, at fixed stellar mass, the only galaxy property that shows correlations with color gradient is the half-light radius $R50$. As pointed out in Paper I, this result suggests that color gradient is related to the surface stellar mass density. On the other hand, previous studies of galaxy clustering and environment have clearly established that stellar mass and color are the galaxy properties most related to environment (e.g. Kauffmann et al. 2004; Blanton & Moustakas 2009) and clustering (e.g. Li et al. 2006a), and that structural parameters such as concentration and surface mass density are less related.

This is all in very good agreement with our findings in this work. We see a strong dependence of clustering on the B-band absolute magnitude and stellar mass, as well as no residual dependence on color gradient when stellar mass is fixed. Therefore, the clustering measurements presented in the current paper reinforce our conclusion from Paper I that the color gradient of a galaxy is related to the structural parameters (e.g. surface mass density), an effect which is independent from the correlation of both properties with stellar mass. The non-dependence of clustering on color gradient is very likely a natural result of the intrinsic relationship between color gradient and galaxy structure. More works are needed in order to better understand this relation, both observationally and theoretically.

Finally, we would like to note that some recent studies (e.g. Liu et al. 2016, 2017) reveal the importance of dust attenuation on color gradients at intermediate to

high redshifts. The effect of dust attenuation should be carefully taken into account when determining color gradients for galaxies at those redshifts. We will come back to this point in future studies.

Acknowledgements This work is supported by the National Key Basic Research Program of China (No. 2015CB857004), the National Key Basic Research and Development Program of China (No. 2018YFA0404502) and NSFC (Grant Nos. 11173045, 11233005, 11325314 and 11320101002). This paper uses data from the VIMOS Public Extragalactic Redshift Survey (VIPERS). VIPERS has been performed using the ESO Very Large Telescope, under the "Large Programme" 182.A-0886. The participating institutions and funding agencies are listed at *http://vipers.inaf.it/*. This paper is based on observations obtained with MegaPrime/MegaCam, a joint project of CFHT and CEA/IRFU, at the Canada-France-Hawaii Telescope (CFHT) which is operated by the National Research Council (NRC) of Canada, the Institut National des Science de l'Univers of the Centre National de la Recherche Scientifique (CNRS) of France, and the University of Hawaii. This research makes use of the VIPERS-MLS database, operated at CeSAM/LAM, Marseille, France. This work is based in part on observations obtained with WIRCam, a joint project of CFHT, Taiwan, Korea, Canada and France. This work is also based in part on observations made with the *Galaxy Evolution Explorer* (*GALEX*). *GALEX* is a NASA Small Explorer, whose mission was developed in cooperation with the Centre National d'Etudes Spatiales (CNES) of France and the Korean Ministry of Science and Technology. *GALEX* is operated for NASA by the California Institute of Technology under NASA contract NAS5-98034. In addition, this work is based in part on data products produced at TERAPIX available at the Canadian Astronomy Data Centre as part of the Canada-France-Hawaii Telescope Legacy Survey, a collaborative project of NRC and CNRS. The TERAPIX team has performed the reduction of all the WIRcam images and the preparation of the catalogs matched with the T0007 CFHTLS data release.

References

Barrow, J. D., Bhavsar, S. P., & Sonoda, D. H. 1984, MNRAS, 210, 19P

Blanton, M. R., & Moustakas, J. 2009, ARA&A, 47, 159

Bundy, K., Bershady, M. A., Law, D. R., et al. 2015, ApJ, 798, 7

Colless, M., Dalton, G., Maddox, S., et al. 2001, MNRAS, 328, 1039

Cuillandre, J.-C. J., Withington, K., Hudelot, P., et al. 2012, in Proc. SPIE, 8448, Observatory Operations: Strategies, Processes, and Systems IV, 84480M

de la Torre, S., Guzzo, L., Peacock, J. A., et al. 2013, A&A, 557, A54

Ferreras, I., Lisker, T., Pasquali, A., Khochfar, S., & Kaviraj, S. 2009, MNRAS, 396, 1573

Goddard, D., Thomas, D., Maraston, C., et al. 2017, MNRAS, 465, 688

Goto, T., Yamauchi, C., Fujita, Y., et al. 2003, MNRAS, 346, 601

Guo, H., Zehavi, I., Zheng, Z., et al. 2013, ApJ, 767, 122

Guzzo, L., Scodeggio, M., Garilli, B., et al. 2014, A&A, 566, A108

Ilbert, O., Tresse, L., Zucca, E., et al. 2005, A&A, 439, 863

Kauffmann, G., White, S. D. M., Heckman, T. M., et al. 2004, MNRAS, 353, 713

Ko, J., & Im, M. 2005, Journal of Korean Astronomical Society, 38, 149

Kovač, K., Lilly, S. J., Knobel, C., et al. 2010, ApJ, 718, 86

La Barbera, F., de Carvalho, R. R., Gal, R. R., et al. 2005, ApJ, 626, L19

La Barbera, F., Ferreras, I., de Carvalho, R. R., et al. 2011, ApJ, 740, L41

Landy, S. D., & Szalay, A. S. 1993, ApJ, 412, 64

Li, C., Kauffmann, G., Heckman, T. M., Jing, Y. P., & White, S. D. M. 2008a, MNRAS, 385, 1903

Li, C., Kauffmann, G., Heckman, T. M., White, S. D. M., & Jing, Y. P. 2008b, MNRAS, 385, 1915

Li, C., Kauffmann, G., Jing, Y. P., et al. 2006a, MNRAS, 368, 21

Li, C., Kauffmann, G., Wang, L., et al. 2006b, MNRAS, 373, 457

Liang, Z.-X. & Li, C., 2018, RAA (Research in Astronomy and Astrophysics), 18, 143 (Paper I)

Liu, F. S., Jiang, D., Guo, Y., et al. 2016, ApJ, 822, L25

Liu, F. S., Jiang, D., Faber, S. M., et al. 2017, ApJ, 844, L2

Madgwick, D. S., Hawkins, E., Lahav, O., et al. 2003, MNRAS, 344, 847

Martin, D. C., Fanson, J., Schiminovich, D., et al. 2005, ApJ, 619, L1

Marulli, F., Bolzonella, M., Branchini, E., et al. 2013, A&A, 557, A17

Meneux, B., Guzzo, L., Garilli, B., et al. 2008, A&A, 478, 299

Meneux, B., Guzzo, L., de la Torre, S., et al. 2009, A&A, 505, 463

Moutard, T., Arnouts, S., Ilbert, O., et al. 2016a, A&A, 590, A102

Moutard, T., Arnouts, S., Ilbert, O., et al. 2016b, A&A, 590, A103

Noll, S., Burgarella, D., Giovannoli, E., et al. 2009, A&A, 507, 1793
Norberg, P., Baugh, C. M., Hawkins, E., et al. 2002, MNRAS, 332, 827
Oke, J. B., & Gunn, J. E. 1983, ApJ, 266, 713
Peebles, P. J. E. 1980, The Large-scale Structure of the Universe (Princeton University Press)
Saglia, R. P., Maraston, C., Greggio, L., Bender, R., & Ziegler, B. 2000, A&A, 360, 911
Schlegel, D. J., Finkbeiner, D. P., & Davis, M. 1998, ApJ, 500, 525
Scodeggio, M., Guzzo, L., Garilli, B., et al. 2018, A&A, 609, A84
Spolaor, M., Kobayashi, C., Forbes, D. A., Couch, W. J., & Hau, G. K. T. 2010, MNRAS, 408, 272
Tamura, N., & Ohta, K. 2000, AJ, 120, 533
Thibault, S., Cui, Q., Poirier, M., et al. 2003, in Proc. SPIE, 4841, Instrument Design and Performance for Optical/Infrared Ground-based Telescopes, eds. M. Iye & A. F. M. Moorwood, 932
Tortora, C., & Napolitano, N. R. 2012, MNRAS, 421, 2478
Wang, L., Li, C., Kauffmann, G., & De Lucia, G. 2007, MNRAS, 377, 1419
Wang, Y., Yang, X., Mo, H. J., et al. 2008, ApJ, 687, 919
White, S. D. M., Tully, R. B., & Davis, M. 1988, ApJ, 333, L45
Willmer, C. N. A., da Costa, L. N., & Pellegrini, P. S. 1998, AJ, 115, 869
York, D. G., Adelman, J., Anderson, Jr., J. E., et al. 2000, AJ, 120, 1579
Zehavi, I., Zheng, Z., Weinberg, D. H., et al. 2005, ApJ, 630, 1
Zehavi, I., Zheng, Z., Weinberg, D. H., et al. 2011, ApJ, 736, 59
Zheng, Z., Wang, H., Ge, J., et al. 2017, MNRAS, 465, 4572